Physica 113B (1982) 299–316
North-Holland Publishing Company

BRILLOUIN-SCATTERING STUDY OF THE STATIONARY, ELECTRO-ACOUSTICALLY AMPLIFIED ACOUSTIC FLUX IN CdS

W. WESTERA

Physics Laboratory, State University of Utrecht, Princetonplein 5, P.O. Box 80 000, 3508 TA Utrecht, The Netherlands

Received 19 January 1982

We investigated the acoustic-energy density of electro-acoustically amplified transverse off-axis waves in single crystals of semiconducting CdS in the frequency range 0.25–1.8 GHz with the help of a Brillouin-scattering technique. The electric field was applied parallel to the c-axis in pulses of 40 μs duration with a rise-time of about 5 μs. The repetition rate was 4 Hz. The excited acoustic flux appeared to be stationary about 5 μs after the onset of the bias pulse. All measurements were carried out at room temperature. The conductivities of the various samples ranged from 0.66 Ω^{-1} m^{-1} to 2.3 Ω^{-1} m^{-1}. The spectral acoustic-energy distribution appeared to peak at a frequency considerably lower than that predicted by White's linear small-signal gain theory. With increasing voltage this peak was found to shift towards lower frequencies, which could be as much as 4 times lower than predicted by White's theory. This down-shift with increasing voltage was discussed in terms of an adapted linear theory: we took into account acoustic-scattering losses at the crystal side-faces and a decrease of the conductivity. The latter effect is thought to be caused by the trapping of free charge carriers in deep potential troughs which are associated with the amplified acoustic waves. We found that the down-shift of the peak frequency with increasing voltage can be described quite well by this adapted linear theory.

The off-axis angle of maximum acoustic-energy density as obtained from Brillouin-scattering experiments appeared to be in good agreement with the off-axis angle as calculated from resonances in the ac impedance.

1. Introduction

Amplification of travelling acoustic waves as a result of their interaction with supersonically drifting charge carriers in piezoelectric semiconductors has been a subject of continuous interest for many years. Many authors [1–16] have used the technique of Brillouin-scattering, i.e. inelastic scattering of light by acoustic waves, for the study of the electro-acoustically excited acoustic flux, as this technique provides a unique tool for the investigation of plane-wave components in a complex acoustic-wave distribution. The electro-acoustically excited flux in piezoelectric semiconductors has usually been found to be concentrated in macroscopic travelling domains starting at the carrier-injecting contact and propagating with the sound velocity in the direction of carrier drift. The occurrence of such travelling acoustic domains involves macroscopic electrical current oscillations with a period equal to the domain transit-time, and a highly nonuniform distribution of the electric field. So far most Brillouin-scattering studies reported in the literature have focussed on the growth of the acoustic flux in these domains. The frequencies of maximum acoustic amplification have been found to be [2, 5–7, 14] an order of magnitude lower than predicted by the linear theory of electro-acoustic amplification, given by White [17] in 1962. Several authors [1, 6, 10–12] have attributed the failure of this linear theory to the occurrence of essential nonlinearities in the interaction between strain waves and space-charge waves. The observed down-shift of the frequency of maximum amplification is thus thought to be caused by parametric down-conversion of the acoustic waves. Yamada et al. [10–12] have observed both down-conversion and up-conversion in the amplified acoustic flux in CdS, which indicates that

0378-4363/82/0000–0000/$2.75

nonlinear frequency mixing may indeed play an important role. Others [5, 14], however, have argued that the trapping of free charge carriers in deep potential troughs that are associated with the amplified acoustic waves is responsible for the observed down-shift with increasing acoustic flux intensities, i.e. with increasing electric field strengths. They have proposed that the electro-acoustic amplification can still be described by the linear theory, if the reduction in the free charge-carrier concentration is taken into account. Since according to White's theory [17] the frequency of maximum amplification was predicted to be proportional to the square root of the free carrier concentration, the trapping of free carriers should indeed result in a down-shift.

Brillouin-scattering data on the amplified acoustic flux without the occurrence of travelling acoustic domains have been reported by Zemon et al. [2] in CdS. The amplified acoustic flux again appeared to be located around frequencies considerably lower than predicted by the linear theory. However, Zemon et al. [2] could not make a quantitative comparison with the linear theory applicable to samples with uniform conductivities only, because this condition was not met in their samples.

The formation of travelling acoustic domains is probably due to shock excitation, caused by the application of short rise-time electrical bias pulses (rise-times $< 1\,\mu$s) [2, 8, 18]. Domain formation can be suppressed by using bias pulses with relatively long rise-times ($>1\,\mu$s); some authors [19, 20] have argued that the use of relatively short samples ($\leqslant 3$ mm) may also be helpful in avoiding domain formation. In the absence of these travelling acoustic domains the acoustic flux will be built up by the amplification of acoustic waves originating from the thermal background [2, 8, 19, 20].

We want to prevent the occurrence of these travelling acoustic domains in our study, as it involves the injection of a large, poorly defined acoustic disturbance. Many et al. [8] have observed that the down-shift of the peak frequency of the acoustic flux within a domain is much more pronounced than in cases where no domains occur. They have proposed that the parametric down-conversion of the acoustic waves is strongly stimulated by the shock-excited flux, the latter acting as the stimulating signal [3]. Therefore the effects of nonlinear frequency mixing may be of importance mainly in acoustic domains. If the acoustic flux is continuously distributed over the sample, i.e. in the absence of domains, the down-shift may possibly be described by the linear theory, in the sense indicated above.

The aim of this paper is to present an extended set of experimental data on the continuously distributed amplified acoustic flux in CdS. We shall discuss experimental data in terms of the linear theory, taking the reduction of the free carrier concentration into account. In section 2 we shall review the results of this theory and summarize the Brillouin-scattering formulas from the literature. In section 3 the scattering configuration and experimental arrangement will be described. Experimental Brillouin-scattering data will be presented in section 4. In section 5 conclusions will be summarized.

2. Theory

In section 2.1 we summarize some theoretical results concerning the description of electro-acoustic effects. In section 2.2 a brief review of Brillouin scattering is given.

2.1. Electro-acoustic attenuation

Although the electro-acoustic effect refers to the *amplification* of acoustic waves, White [17] would have preferred the term *attenuation*, because the process of amplification (negative attenuation) can be regarded as anomalous behaviour. In some cases, however, the term attenuation is quite confusing. In this paper we shall use both the term amplification and the

term (negative) attenuation, giving some preference to the latter.

In [21] we presented a theoretical model for the description of electro-acoustic current saturation, current noise and ac-impedance effects in an n-type piezoelectric semiconductor where the electric field is parallel to the c-axis. These electro-acoustic effects arise essentially from nonlinearities in the interaction between free charge carriers and amplified acoustic waves. To avoid the need for nonlinear equations we have assumed that the observed electro-acoustic effects can be described by the random trapping and de-trapping of free charge carriers in potential troughs. These potential troughs are associated with the amplified acoustic waves. In fact, the *cause* of potential troughs (i.e. the amplified acoustic flux) has been disregarded in the theoretical description; only the *effect* of the flux (i.e. potential troughs) has been taken into account. We could do this only if we made certain assumptions about the properties of these troughs. It should be noted that the current noise and ac-impedance effects usually occur at frequencies far below the frequencies of the amplified acoustic waves [20, 22, 23]. Although this model is a much simplified representation of the complex electro-acoustic effects, its theoretical predictions appeared to be consistent with the experimental current-noise and ac-impedance data [22, 23]. This trough model has also been used to derive expressions for the wave attenuation coefficients [21]. Experimental data on the frequency distribution of the acoustic energy, which are presented here, are connected in some way with the wave attenuation coefficients.

The expressions for the wave attenuation coefficients obtained with the potential-trough model contain various parameters; these include parameters related to the electric field dependence of the potential-trough creation and annihilation rates, potential-trough lifetimes, parameters related to electro-acoustic dispersion, etc. [21]. As we pointed out before [22, 23], these parameters, which are obtained from current-noise and ac-impedance data, cannot be determined very accurately. Due to these inaccuracies the frequency and voltage dependence of the associated wave attenuation coefficients cannot be determined unambiguously. Besides, it is doubtful whether the potential-trough model still holds at frequencies close to the frequencies of the amplified acoustic waves. For these reasons we prefer to discuss our Brillouin-scattering results not in terms of the previously published potential-trough model, but rather in terms of White's linear small-signal gain theory, taking a reduction of the free carrier concentration into account.

According to the potential-trough model [21] electrons become trapped in potential troughs and thereby can no longer participate in the sound-amplification process. The remaining average free electron conductivity, denoted by σ_1, can be calculated at each applied electric field strength from the measured plateau-value Z_{pl} of the ac impedance [23] by using

$$\sigma_1 = \frac{L}{AZ_{pl}}, \tag{1}$$

where L is the contact spacing, and A is the cross-sectional area. Instead of using the Ohmic conductivity, as did White [7] to calculate the electro-acoustic attenuation coefficients, we consider it more appropriate to use the reduced conductivity σ_1. It should be noted that generally Z_{pl} is found to differ from the differential resistance as obtained from the current–voltage characteristic [23].

Once the reduction of the free carrier concentration resulting from nonlinear effects has been taken into account, it is assumed that the amplification of acoustic waves under current-saturation conditions can be described by the linear theory.

According to the modified linear theory the electro-acoustic attentuation coefficient α_e for an acoustic wave of frequency ω having an off-axis

angle δ (the angle between the acoustic wave-vector and the c-axis) is given by [17, 24, 25]

$$\alpha_e(\omega, \delta) = \frac{K_e^2(\delta)}{2v_{so}(\delta)} \frac{\gamma\omega_c'}{\gamma^2 + (\omega_c'/\omega + \omega/\omega_D)^2}, \quad (2)$$

where K_e is the electro-mechanical coupling factor, v_{so} is the unstiffened acoustic phase velocity, $\omega_c' = \sigma_1/\varepsilon$ is the modified angular dielectric-relaxation frequency, ε is the permittivity of the material, $\gamma = 1 - \bar{v}_d \cos\delta/v_s$ is the drift parameter, $\bar{v}_d$ is the electron drift-velocity, v_s is the stiffened acoustic phase velocity (slightly different from v_{so}), $\omega_D = v_s^2/D_n$ is the angular electron-diffusion frequency, and D_n is the electron-diffusion constant.

Amplification occurs if α_e is negative. This happens when the drift parameter γ is negative, i.e. when the component of the drift velocity $\boldsymbol{v}_d$ along the acoustic phase velocity $\boldsymbol{v}_s$ exceeds v_s. From eq. (2) we find that maximum amplification occurs at an angular frequency given by

$$\omega = \omega_m \equiv (\omega_D\omega_c')^{1/2}. \quad (3)$$

The frequency of maximum sound amplification is thus found to be directly proportional to the square root of the free electron conductivity σ_1. Since the ac-impedance plateau-value Z_{pl} is usually found to increase monotonically with increasing applied voltage [23], this modified linear theory predicts a down-shift of ω_m with increasing voltage (cf. eq. (1)).

It should be noted that the expression for the attenuation coefficients obtained from the potential-trough model [21] reduces to eq. (2) in the extreme limit $1/\tau_1 = 1/\tau_2 = 0$, where τ_1 and τ_2 are mean lifetimes of fluctuations in the numbers of troughs. Physically this means that no trapping and de-trapping occur. However, it should be noted that expression (2) cannot be derived from the potential-trough model by putting only $\omega\tau_1 \gg 1$ and $\omega\tau_2 \gg 1$.

In practice the net amplification of acoustic waves will be reduced somewhat due to the occurrence of lattice attenuation. Lattice attenuation has been studied extensively in CdS [9, 11, 26–31]. Several authors [9, 30, 31] have found experimentally that electro-acoustically amplified acoustic waves originating from the thermal background undergo lattice attenuation which is proportional to ω^2. Thus, the lattice attenuation coefficient α_L can be written as

$$\alpha_L = A_0\omega^2, \quad (4)$$

where A_0 is a material constant. These results are in accordance with the theoretical predictions of Akhiezer [32].

In addition a second loss process may be of importance: in most practical cases off-axis waves will suffer from acoustic losses due to scattering at the crystal side-faces. This effect can formally be taken into account by introducing an attenuation coefficient α_S. Yamada et al. [11] showed that α_S can be written as

$$\alpha_S = \frac{2\pi s^2\omega^2}{\sqrt{A}v_s^2(\delta)} \sin^2\delta, \quad (5)$$

where s is a measure for the surface flatness. Experimental observations have been found to be in agreement with eq. (5) [11]. Since this attenuation coefficient is proportional to $\sin^2\delta/v_s^2(\delta)$, and $v_s(\delta)$ is only weakly dependent on δ, boundary-scattering losses become more important with increasing off-axis angle δ.

The net attenuation coefficient α_N is given by

$$\alpha_N = \alpha_e + \alpha_L + \alpha_S, \quad (6)$$

and shows a frequency and angular dependence which is different from that of α_e (cf. eq. (1)).

As we pointed out before [21, 23], resonances appearing in the ac impedance can be used to estimate the off-axis angle of maximum sound amplification. Resonances appear in the ac impedance at frequencies given by

$$f = f_l = \frac{(2l+1)}{2}\frac{v_{g_3}}{L}; \qquad l = 0, 1, 2, 3, \ldots \tag{7}$$

where v_{g_3} is the component of the acoustic group velocity along the c-axis. As a result of the elastic anisotropy in CdS the direction and magnitude of the group velocity may differ markedly from the direction and magnitude of the phase velocity. However, from the value of v_{g_3}, obtained with eq. (7), we can calculate the associated off-axis angle of maximum sound amplification unambiguously, if the values of the elastic constants are known. Thence, the off-axis angle of maximum amplification can be obtained in two independent ways: from Brillouin scattering as well as from ac-impedance measurements.

2.2. Brillouin scattering

If the inter-atomic distance in a medium is small compared to the optical wavelength, the theory of light scattering can be given in a classical continuum description. It can be shown that the scattering of light in dielectric media is caused by local fluctuations in the dielectric properties, or rather by local fluctuations in the refractive properties [33, 34]. In a thermodynamical treatment these fluctuations are thought to be caused by non-propagating temperature fluctuations [33–35] and by propagating strain fluctuations [36]. The non-propagating fluctuations produce quasi-elastically scattered radiation with a central frequency equal to that of the incident radiation. The frequency width of this quasi-elastic scattering is determined by the mean lifetime of the scattering fluctuations. The propagating fluctuations give rise to a Brillouin doublet, located approximately symmetrically on either side of the unshifted line and separated from it by a frequency interval equal to the frequency of the propagating strain wave. The presence of this doublet was predicted by Brillouin [37] in 1922, and first observed by Gross [38] in 1930. The linewidth of the Brillouin doublet is determined by the mean lifetime of the scattering strain waves. The intensity of the Brillouin-scattered light is directly related to the energy density of the scattering strain wave.

The use of Brillouin scattering as an optical probe for studying the electro-acoustically excited acoustic flux requires detailed knowledge of the kinematics of the scattering process, and the scattering efficiency.

In optically isotropic media the kinematics of the scattering process is conditioned by the normal Bragg condition. The scattering geometry in optically anisotropic media such as CdS is determined by the generalized Bragg relations, first derived by Dixon [39]. These relations can be derived from the conservation laws for energy and pseudo-momentum. Let $\boldsymbol{k}_{in}$ be the wave vector of the monochromatic, plane polarized incident light inside the medium (angular frequency ω_{in}), $\boldsymbol{k}_{sc}$ the wave vector of the scattered light (angular frequency ω_{sc}) and $\boldsymbol{k}$ that of the acoustic wave (angular frequency ω). Then the conservation laws for the anti-Stokes process read (cf. fig. 1)

$$\boldsymbol{k}_{in} + \boldsymbol{k} = \boldsymbol{k}_{sc}, \tag{8}$$

$$\omega_{in} + \omega = \omega_{sc}. \tag{9}$$

Note that eqs. (8) and (9) only hold for a single scattering process. As the scattering is only weak in our experiments, multiple scattering can be neglected. In this paper we restrict ourselves to

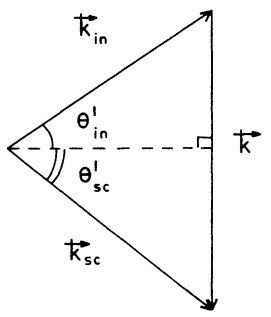

Fig. 1. Schematic diagram showing the wave-vector construction for an anti-Stokes process. The figure also serves to define the angles θ'_{in} and θ'_{sc}.

the formulas for the anti-Stokes process. Similar relations apply to the Stokes process [36, 39, 49].

From eqs. (8) and (9) we obtain the following relations for the angles shown in fig. 1 (if $\omega \ll \omega_{in}$):

$$\sin\theta'_{in} = \frac{\lambda_0}{2n_{in}v_s}\left[f + \frac{v_s^2}{f\lambda_0^2}(n_{in}^2 - n_{sc}^2)\right], \tag{10}$$

$$\sin\theta'_{sc} = \frac{\lambda_0}{2n_{sc}v_s}\left[f - \frac{v_s^2}{f\lambda_0^2}(n_{in}^2 - n_{sc}^2)\right]. \tag{11}$$

Here v_s is the phase velocity and $f = \omega/2\pi$ the frequency of the acoustic wave, λ_0 the wavelength of the incident light in free space, and n_{in} and n_{sc} are the polarization-dependent refractive indices for the incident and scattered light, respectively. Note that θ'_{in} and θ'_{sc} are angles inside the medium.

Expressions (10) and (11) are known as the generalized Bragg relations. In the isotropic case ($n_{in} = n_{sc}$) these relations reduce to the well-known normal Bragg relation (corresponding to first-order diffraction):

$$\sin\theta'_{in} = \sin\theta'_{sc} = \frac{\lambda_0 f}{2n_{in}v_s}. \tag{12}$$

From eqs. (10) and (11) we find an upper limit for the acoustic frequency, above which no Brillouin scattering occurs. This upper limit is given by

$$f_{max} = \frac{v_s}{\lambda_0}(n_{in} + n_{sc}), \tag{13}$$

which holds for the case of collinear interaction with $\theta'_{in} = \theta'_{sc} = \pi/2$. For example, let $n_{in} = n_\perp$ and $n_{sc} = n_\parallel$, where $n_\perp$ and $n_\parallel$ are the refractive indices for light polarized perpendicular to and parallel to the c-axis respectively. Then, using $\lambda_0 = 632.8$ nm, $v_s \simeq 2 \times 10^3$ m s^{-1}, $n_\perp = 2.453$ and $n_\parallel = 2.471$ [4], $f_{max} \simeq 15$ GHz for transverse waves in CdS. Furthermore, in the anisotropic case a lower limit for the acoustic frequency, below which no interaction occurs, is given by

$$f_{min} = \frac{v_s}{\lambda_0}|n_{in} - n_{sc}|. \tag{14}$$

This case corresponds to the collinear interaction with $\theta'_{in} = -\theta'_{sc}$ and $|\theta'_{in}| = |\theta'_{sc}| = \pi/2$. In CdS $f_{min} \approx 57$ MHz for transverse waves. Note that in the isotropic case there is no positive low-frequency limit.

Once the angles θ'_{in} and θ'_{sc} have been chosen, the frequency f of the acoustic waves that are to be investigated by Brillouin scattering is uniquely determined by the generalized Bragg relations. Thus the adjustment of θ'_{in} and θ'_{sc} provides a simple tool for the selection of the acoustic wave-vector to be studied. To be useful in the experiment the internal angles θ'_{in} and θ'_{sc} should be translated into external angles. This translation for our particular geometrical conditions will be carried out in section 3.

Recently Mishra and Bray [41] have established that the power of Brillouin-scattered light provides a linear measure for the acoustic-energy density, even in the case of the very intense acoustic flux which is generally attained in electro-acoustically active crystals. Because the acoustic-energy density of thermal waves is known, the measurement of the power of the light scattered by these thermal waves would provide an absolute calibration of the measured acoustic-energy density. However, the sensitivity of the experimental set-up (cf. section 3) did not allow the measurement of the light power scattered by thermal acoustic waves. Yet, the power scattered by electro-acoustically amplified waves could still be compared with the power scattered by thermal waves, because the latter is known theoretically. This enabled us to give absolute values for the measured acoustic-energy densities.

The efficiency of Brillouin scattering by thermal strain waves has been calculated by Benedek and Fritsch [36] for the case of cubic crystals. Hamaguchi [40] extended the calculation to the

case of crystals with hexagonal symmetry. In these calculations it was assumed that the dielectric fluctuations are linearly related to fluctuations in the strain. The coefficients in this linear relationship are known as the photoelastic, elasto-optical or Pöckels-tensor elements p_{ijkl} (the subscripts i, j, k and l run from 1 to 3).

Let the power of the incident radiation be P_0; the power dP_{th} of the radiation scattered by thermal acoustic waves while it travels over the path-length l, into an internal solid angle $d\Omega'$, is then given by

$$dP_{th} = P_0 \sigma_{th} l \, d\Omega' \beta , \tag{15}$$

where σ_{th} is the scattering efficiency per unit length per (internal) unit solid angle; β is a factor describing the influence of the attenuation of the incident and scattered radiation by absorption and scattering inside the medium, and by reflection at the crystal boundaries. This factor will be discussed in section 3.4. In the range of acoustic frequencies much smaller than $k_B T/h$, where k_B is Boltzmann's constant, T is temperature and h is Planck's constant, the scattering efficiency σ_{th} for a Stokes or an anti-Stokes process is given by [40]:

$$\sigma_{th} = \frac{\pi^2 k_B T}{2\lambda_0^4 \rho v_s^2} |\boldsymbol{\xi}|^2 . \tag{16}$$

Here ρ is the mass density of the medium and $\boldsymbol{\xi}$ is a vector which determines explicitly the polarization of the scattered light. When $\boldsymbol{\pi}$ is a unit vector indicating the polarization of the sound wave, $\boldsymbol{p}_{in}$ a unit vector indicating the polarization of the incident radiation, $\boldsymbol{\kappa} = \boldsymbol{k}/|\boldsymbol{k}|$ is a unit vector along the acoustic wave vector and $\boldsymbol{\kappa}_{sc} = \boldsymbol{k}_{sc}/|\boldsymbol{k}_{sc}|$ is a unit vector along the wave vector of the scattered light, the vector $\boldsymbol{\xi}$ is given by

$$\boldsymbol{\xi} = \boldsymbol{\kappa}_{sc} \times (\boldsymbol{\kappa}_{sc} \times \boldsymbol{\eta}) , \tag{17}$$

where

$$\eta_i = \frac{\varepsilon_{ii}}{\varepsilon_0^2} \sum_{j,k,l=1}^{3} \varepsilon_{jj} p_{ijkl} p_{in_j} \kappa_{sc_k} \pi_l \qquad (i = 1, 2, 3) , \tag{18}$$

where ε_0 is the vacuum permittivity. Note that generally $\boldsymbol{\xi}$ is not a unit vector.

Now, by measuring the power dP of the light scattered by the geometrically selected acoustic waves, we can calculate the spectral acoustic-energy density w per unit solid angle of these waves with the help of the equation

$$w = \frac{dP}{dP_{th}} w_{th} , \tag{19}$$

where w_{th} is the acoustic energy per unit frequency per unit volume per unit solid angle of thermal waves; this is given by

$$w_{th} = f^2 k_B T / v_s^3 . \tag{20}$$

By substituting eqs. (15), (16) and (20) into eq. (19) we find

$$w = \left(\frac{dP}{P_0}\right) \frac{2\rho\lambda_0^4 f^2}{\pi^2 \beta |\boldsymbol{\xi}|^2 l \, d\Omega'} . \tag{21}$$

3. Experimental arrangements

In section 3.1 we shall specify the characteristics of the samples used in the experiments. In section 3.2 the experimental set-up is described. In section 3.3 we discuss the scattering configuration. In section 3.4 some correction formulas are given. In section 3.5 we present some estimates of the acoustic wave-vector resolution.

3.1. The samples

For our experiments we used semiconducting single crystals of hexagonal n-type CdS obtained from Eagle Picher Industries, Inc. To make Brillouin-scattering experiments possible two opposite side-faces were mechanically polished

to a flatness of about $\frac{1}{4}$ μm. In some cases the two other side-faces or the two contact faces were polished as well. Unpolished surfaces, being several orders of magnitude less flat than polished ones, can be expected to cause considerable acoustic scattering losses, since the wavelengths of the amplified acoustic waves, having frequencies around 1 GHz, are about 2 μm [24].

The samples were supplied with two In-evaporated ohmic contacts in such a way that the electric field was orientated along the c-axis (the longitudinal configuration). The In-contacts covered the end-surfaces completely. For details we refer to [23].

In table I the dimensions, dark-conductivity at room temperature and surface characteristics of the samples have been listed. Data on current saturation, ac impedance and current noise for samples s_3, s_4 and s_5 have been presented in [22, 23].

3.2. Experimental set-up

In the Brillouin-scattering experiments we selected acoustic wave vectors directed parallel to the polished crystal side-faces (cf. fig. 2). Then, the internal angles θ'_{in} and θ'_{sc} are related to the external angles θ_{in} and θ_{sc} by Snell's law as follows:

$$\sin \theta_{in} = n_{in} \sin \theta'_{in} , \tag{22}$$

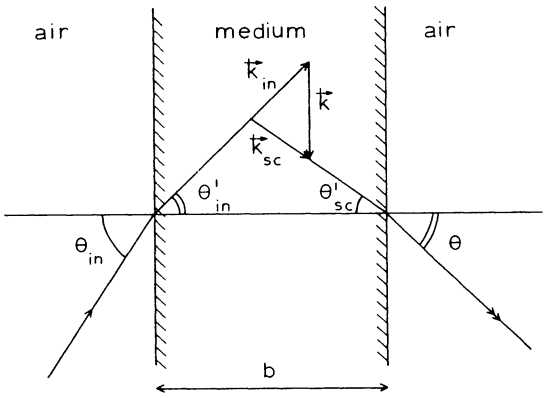

Fig. 2. Refraction of the incident and scattered light at the medium/air interfaces. The selected acoustic wave-vector was always parallel to the side-faces.

$$\sin \theta_{sc} = n_{sc} \sin \theta'_{sc} . \tag{23}$$

Note that for this geometry the operational frequency-interval suitable for Brillouin-scattering experiments, which is related to the limiting frequencies f_{min} and f_{max} (cf. eqs. (13) and (14)), is reduced due to the occurrence of total internal reflections. From fig. 2 we find that the path-length l, as occurring in eq. (15), is equal to $b/\cos \theta'_{in}$, where b is the sample thickness.

To avoid excessive Joule heating of the samples the voltage was applied in pulses of 40 μs with a repetition rate of 4 Hz. The duration of these pulses was sufficient for the samples to reach a stationary state. To suppress travelling acoustic-domain formation we used rise-times of

Table I
Characteristics of the CdS samples

Sample	L (mm)	A (mm^2)	Dark-conductivity at room temp. (Ω^{-1} m^{-1})	Polished faces (mm^2)
s_3	1.63	1.78 × 0.48	0.95	1.78 × 1.63-faces 1.78 × 0.48-faces
s_4	1.76	1.24 × 0.43	0.66	1.24 × 1.76-faces
s_5	2.79	1.43 × 0.37	2.3	all faces
s_7	1.96	1.99 × 0.58	1.4	1.99 × 1.96-faces 1.96 × 0.58-faces

about 5 μs. Under these conditions only a continuous type of acoustic flux was amplified.

The height of the voltage pulses was measured with a sample-and-hold circuit.

The experimental set-up for the Brillouin-scattering experiments was similar to that in the original paper of Zucker et al. [1] (cf. fig. 3). A helium–neon (He–Ne) laser (output $\leqslant 1$ mW; $\lambda_0 = 632.8$ nm) was used as a light source. The laser beam was polarized by a Glan–Thomson prism and focussed to a diameter of about 0.1 mm on the sample. The sample was placed on a translatable and rotatable sample-mount. Light scattered into an external solid angle $d\Omega$, defined by the aperture angle of a circular diaphragm, passed through a collimating lens and a second Glan–Thomson polarizer before it was detected by an EMI 9558 B photomultiplier. The laboratory angles θ_{in} and θ_{sc} could be varied independently to select the acoustic wave-vector. The apparatus needed for the investigation of the scattered light (consisting of a photomultiplier, analyzer, lens and diaphragm) was placed on an optical rail connected to a turntable.

Since the radiation scattered by the electro-acoustically excited flux is present only during the application of the voltage pulse to the sample, it causes a synchronous modulation of the detector current. The quasi-elastically scattered light, mainly resulting from static crystal defects [34] produces a stationary detector current. Thus, the ac part of the detector current provides a measure for the intensity of the light scattered by the amplified acoustic waves. This part of the detector current was measured with a synchronized sample-and-hold circuit and recorded on an *xt*-recorder.

3.3. Scattering configuration

In [23] we pointed out that transverse off-axis waves are amplified in our samples. The polarization vector of these waves lies in the plane through the acoustic wave vector and parallel to the *c*-axis (T_2-mode); T_1-waves (polarization perpendicular to the *c*-axis) produce no piezo-electric fields [24, 25].

To make Brillouin-scattering measurements possible for off-axis angles of up to 30° or more, we used the scattering configuration introduced by San'ya et al. [13] (cf. fig. 4). The sample was mounted on the scattering table in such a way that it could be inclined with respect to the scattering plane. In this way any desirable off-axis angle could be selected.

The polarization of the incident light was

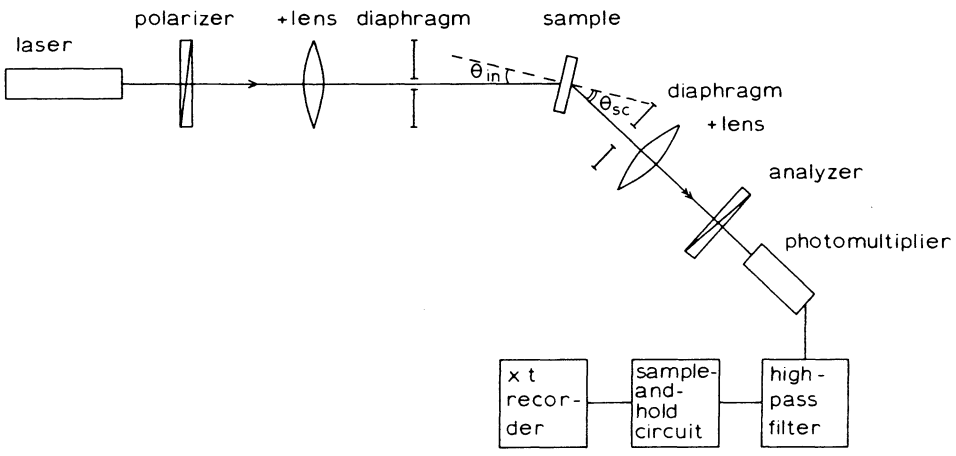

Fig. 3. The experimental set-up for the measurement of Brillouin-scattered light.

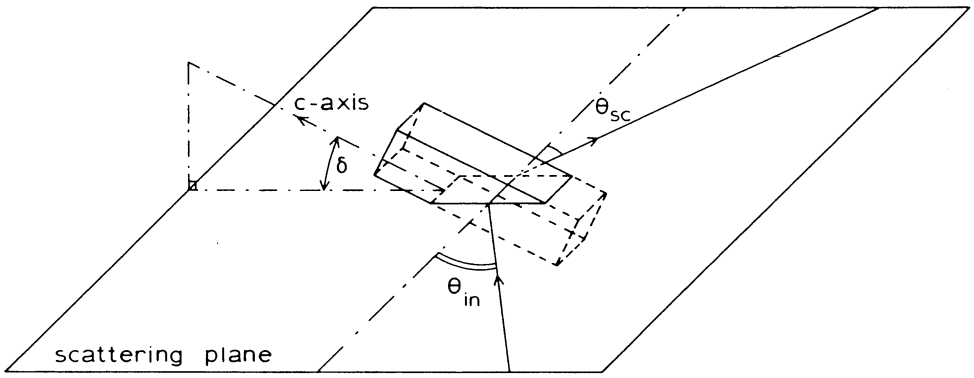

Fig. 4. Brillouin-scattering configuration suitable for the study of off-axis waves.

chosen perpendicular to the c-axis. So we can put

$$n_{in} = n_{\perp} . \tag{24}$$

The Brillouin-scattered light contained various components of polarization, defined by the vector ξ in eq. (17). To minimize the disturbing effect of the quasi-elastically scattered radiation, which in general shows no change of polarization, we detected only the extraordinary component of the Brillouin-scattered light by adjusting the analyzer. It can be shown that the associated extraordinary refractive index is given by [13, 42]:

$$n_{sc} = n_{\perp} n_{\parallel} [n_{\perp}^2 + (n_{\parallel}^2 - n_{\perp}^2) \sin^2 \theta'_{sc} \cos^2 \delta]^{-1/2} . \tag{25}$$

From eqs. (10), (11), (22)–(25) a unique relationship can be obtained between the acoustic frequency f and the laboratory angles θ_{in} and θ_{sc}. Under these conditions we were able to select acoustic waves with frequencies ranging from about 0.25 GHz to 3 GHz, without the angle $|\theta_{in}|$ ever exceeding 25°. Still larger angles of incidence would give rise to an unacceptable reduction in the spatial resolution.

3.4. Scattered power outside the scattering medium

The power of the incident light as well as that of the Brillouin-scattered light may be reduced by scattering and absorption inside the medium. In addition, (multiple) reflections at the air/solid interfaces reduce the power that is received by the detector.

Let $\sigma_{T_{in}}$ be the total scattering coefficient and α_{in} the absorption coefficient of the incident light, respectively; let the corresponding coefficients for the Brillouin-scattered light be denoted by $\sigma_{T_{sc}}$ and α_{sc}. We derived an expression for the correction factor β, introduced in eq. (15), which accounts for the power reduction of the incident and scattered light due to scattering, absorption and multiple reflections. The factor β is given by

$$\begin{aligned}\beta = {} & \left\{ \exp\left[\frac{(\sigma_{T_{sc}} + \alpha_{sc})b}{\cos \theta'_{sc}} - \frac{(\sigma_{T_{in}} + \alpha_{in})b}{\cos \theta'_{in}} \right] - 1 \right\} \\ & \times \exp\left[- \frac{(\sigma_{T_{in}} + \alpha_{in})b}{\cos \theta'_{in}} \right] (1 - R_{in})(1 - R_{sc}) \\ & \times \left[\left\{ \frac{(\sigma_{T_{sc}} + \alpha_{sc})}{\cos \theta'_{sc}} - \frac{(\sigma_{T_{in}} + \alpha_{in})}{\cos \theta'_{in}} \right\} b \right. \\ & \times \left\{ 1 - R_{in}^2 \exp\left(\frac{-2(\sigma_{T_{in}} + \alpha_{in})b}{\cos \theta'_{in}} \right) \right\} \\ & \left. \times \left\{ 1 - R_{sc}^2 \exp\left(\frac{-2(\sigma_{T_{sc}} + \alpha_{sc})b}{\cos \theta'_{sc}} \right) \right\} \right]^{-1} , \end{aligned} \tag{26}$$

where R_{in} and R_{sc} are reflection coefficients given by Fresnel's law [42]. In fact, if the angle be-

tween the polarization vector $\boldsymbol{p}_{in}$ of the incident light and the plane of refraction (or scattering) is denoted by ϕ_{in}, and the angle between the polarization vector $\boldsymbol{p}_{sc}$ of the analysed, scattered light and the refraction plane by ϕ_{sc}, then R_{in} and R_{sc} are given by

$$R_{in} = \frac{\mathrm{tg}^2(\theta_{in} - \theta'_{in})}{\mathrm{tg}^2(\theta_{in} + \theta'_{in})} \cos^2 \phi_{in} + \frac{\sin^2(\theta_{in} - \theta'_{in})}{\sin^2(\theta_{in} + \theta'_{in})} \sin^2 \phi_{in} , \tag{27}$$

$$R_{sc} = \frac{\mathrm{tg}^2(\theta_{sc} - \theta'_{sc})}{\mathrm{tg}^2(\theta_{sc} + \theta'_{sc})} \cos^2 \phi_{sc} + \frac{\sin^2(\theta_{sc} - \theta'_{sc})}{\sin^2(\theta_{sc} + \theta'_{sc})} \sin^2 \phi_{sc} . \tag{28}$$

If we were to omit the effects of reflections at the crystal boundaries by putting $R_{in} = R_{sc} = 0$, eq. (26) would reduce to the result obtained by Ando et al. [43]. In our samples the attenuation of the laser light due to scattering and absorption appeared to be of little importance.

For small cone angles the internal solid angle $\mathrm{d}\Omega'$ is related to the external solid angle $\mathrm{d}\Omega$ by [40]:

$$\mathrm{d}\Omega' = \frac{\cos \theta_{sc}}{n_{sc}(n_{sc}^2 - \sin^2 \theta_{sc})^{1/2}} \mathrm{d}\Omega . \tag{29}$$

If we realize that only the component of $\boldsymbol{\xi}$ parallel to $\boldsymbol{p}_{sc}$ is detected, eq. (21) can be rewritten as (we used eqs. (20) and (29)):

$$w = \frac{\mathrm{d}P}{P_0} \frac{2\rho\lambda_0^4 f^2 n_{sc}(n_{sc}^2 - \sin^2 \theta_{sc})^{1/2} \cos \theta'_{in}}{\pi^2 \beta |\boldsymbol{\xi} \cdot \boldsymbol{p}_{sc}|^2 b \cos \theta_{sc} \, \mathrm{d}\Omega} . \tag{30}$$

The lowest value of w we could measure turned out to be about $5 \times 10^3 \, w_{th}$. This detection limit was set by the noise in the detector current which was due to the intensity of the quasi-elastically scattered light still passing through the crossed polarization filters. However, the energy density of the electro-acoustically amplified acoustic waves was usually much higher than this detection limit.

3.5. Acoustic wave-vector resolution

In our experiments the acoustic wave-vector resolution was limited due to the finite extent of the solid angle $\mathrm{d}\Omega$ of detection. If a wave vector with a frequency f and off-axis angle δ is selected in the way discussed before, acoustic waves with frequencies in the interval $(f \pm \Delta f)$ and off-axis angles in the interval $(\delta \pm \Delta\delta)$ scatter light into the solid angle $\mathrm{d}\Omega$ as well. From geometrical considerations we found the frequency resolution Δf to be given by

$$(\Delta f)^2 \approx \frac{v_s^2}{\lambda_0^2} \frac{\mathrm{d}\Omega}{\pi} . \tag{31}$$

The angular resolution $\Delta\delta$ of acoustic waves is given by

$$\Delta\delta^2 \approx \frac{v_s^2}{f^2 \lambda_0^2} \frac{\mathrm{d}\Omega}{2\pi} . \tag{32}$$

It should be noted that Δf and $\Delta\delta$ are not half-power band-widths, but indicate the maximum deviations from the selected frequency f and off-axis angle δ, respectively.

In our case $\mathrm{d}\Omega$ was always smaller than 1.8×10^{-3} sr. Inserting this value in eq. (31) we obtain $\Delta f \approx 8 \times 10^7$ Hz. The angular resolution $\Delta\delta$ is a function of the acoustic frequency. For $f = 10^9$ Hz we find from eq. (32) that $\Delta\delta \approx 3°$; at $f = 3 \times 10^8$ Hz we even find $\Delta\delta \approx 9°$.

4. Experimental results and discussion

When investigating the propagation characteristics of an acoustic disturbance that is formed by a collection of plane acoustic waves with wave vectors centred in a narrow cone around a certain central wave vector, one should realize that the direction of the acoustic-energy flow is determined by the acoustic group velocity. As a result of the elastic anisotropy in CdS the magnitudes and directions of the group velocity and the phase velocity may be quite different [15].

This elastic dispersion effect is illustrated in fig. 5: an acoustic disturbance originating from 0 will propagate along the direction of the group velocity v_g, if the associated phase velocities are centred around v_s. For instance, for $\delta = 30°$ the angle between the group velocity and the c-axis appears to be 45° in CdS [15].

In preliminary measurements we were able to verify the predicted frequency-shift of the Brillouin-scattered light using a Spectra Physics 470 spectrum analyzer (a Fabry–Perot interferometer).

The possible laser-induced generation of free charge carriers from local centres was investigated by varying the laser-light intensity. Photo-excitation would locally change the electro-acoustic properties of the crystal. The intensities of the incident light in our experiments were always such that the power of the Brillouin-scattered light was proportional to the power of the incident light. From this result we concluded that effects of local photo-excitation could be neglected in our case.

Fig. 6 shows acoustic spectra for sample s_7, at various collinear positions. The selected off-axis angle was 30°; the positions were chosen along the direction of the acoustic energy flow (i.e. at 45°). The position coordinate $r = 0.8$ mm was found to be quite close to the anode. (Note that the origin $r = 0$ was chosen arbitrarily.) The position of the anode could not be determined very accurately due to the finite cross section of the laser beam and to the oblique angles of incidence and scattering. All spectra in fig. 6

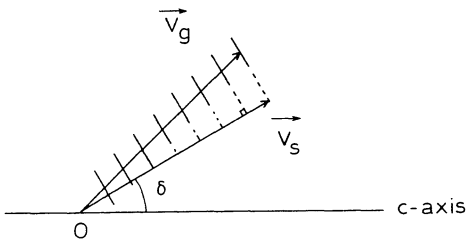

Fig. 5. Elastic dispersion in CdS. v_s is the phase velocity, v_g is the group velocity. Wavefronts are indicated by parallel lines perpendicular to v_s.

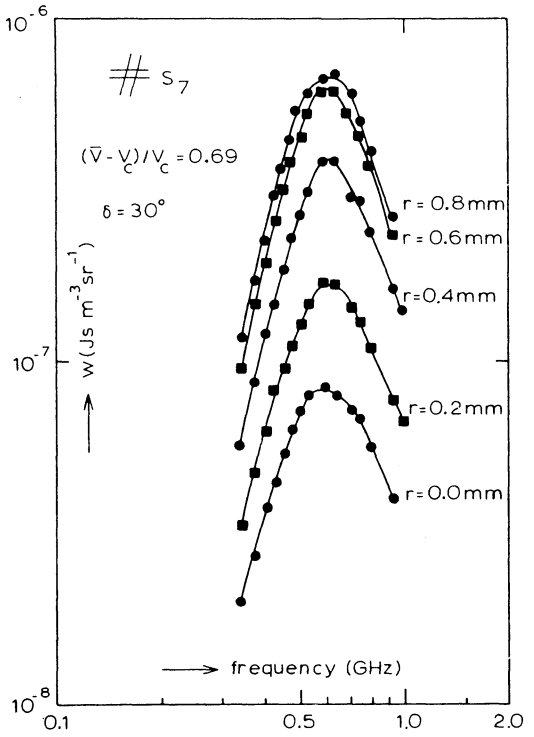

Fig. 6. Acoustic spectra for sample s_7 at various collinear positions. The off-axis angle was 30°. The position vector r was directed along the acoustic group velocity (at 45°). The origin, $r = 0$, was chosen arbitrarily. The position $r = 0.8$ mm is near the anode.

were obtained at the same reduced voltage $(\bar{V} - V_c)/V_c = 0.69$, where $\bar{V}$ is the applied voltage and V_c is the voltage defined by the onset of electro-acoustic current fluctuations [22]. The external solid angle of detection was fixed at 5×10^{-4} sr. The intensity of the Brillouin-scattered light reached a constant level about 5 μs after the onset of the bias pulse. The current and current noise appeared to remain constant after 5 μs as well. These observations indicate that after 5 μs the sample reached a stationary state.

From fig. 6 we observe that the spectral acoustic-energy density increases monotonically the closer one measures to the anode, whereas the shape of the spectra remains almost unchanged. In addition, each spectrum shows a maximum at about 0.6 GHz. It is expected that this frequency will somehow be related to the

frequency of maximum acoustic amplification. To find the latter frequency we should take into account that the number of acoustic modes in the frequency interval between f and $f + \mathrm{d}f$ is proportional to f^2. The frequency of maximum acoustic amplification will coincide with the frequency where a maximum occurs in the quantity $w(f)/f^2$, which is proportional to the acoustic energy of a single acoustic mode. From the data in fig. 6 we derive that the maximum of $w(f)/f^2$ lies at 0.5 GHz. White's theory [17] predicts a maximum at 1.8 GHz, a value too large compared with the measured 0.5 GHz. Better agreement with the theory is obtained if we use eq. (1) combined with eq. (3). Then we find a maximum at 0.95 GHz (using $Z_{pl} = 4.3\,\mathrm{k\Omega}$). Lattice attenuation (cf. eq. (4)) is of little importance. Taking lattice attenuation ($A_0 \simeq 3 \times 10^{-17}\,\mathrm{dB\,s^2\,m^{-1}\,rad^{-2}}$ [29–31]) into account the maximum in the amplification coefficient is still found to be located at 0.95 GHz. The theoretical frequency of maximum net amplification (cf. eq. (6)) can be fitted to the experimental value of 0.5 GHz by inserting a value $s = 0.9\,\mu\mathrm{m}$ for the surface-flatness parameter s (cf. eq. (5)). This value is quite acceptable: in the polishing procedure we used diamond powder with a fineness of about $\frac{1}{4}\,\mu\mathrm{m}$. The value of α_N at 0.5 GHz was found to be $-8.4 \times 10^3\,\mathrm{dB\,m^{-1}}$.

Fig. 7 shows the data of fig. 6 and some supplementary data at 0.5 GHz plotted versus position r. We observe that the local acoustic-energy density varies approximately exponentially with position r. At positions close to the anode ($r = 0.7$–0.8 mm) the acoustic-energy density seems to saturate somewhat. At these positions the incident and scattered light may perhaps have been partially blocked by the anode, resulting in a reduction of the detector current.

We might interpret the exponential position-dependence of the acoustic-energy density as some kind of electro-acoustic attenuation coefficient. From the slope in fig. 7 we obtained an operationally defined negative attenuation coefficient of $-6.9 \times 10^3\,\mathrm{dB\,m^{-1}}$, a value close to

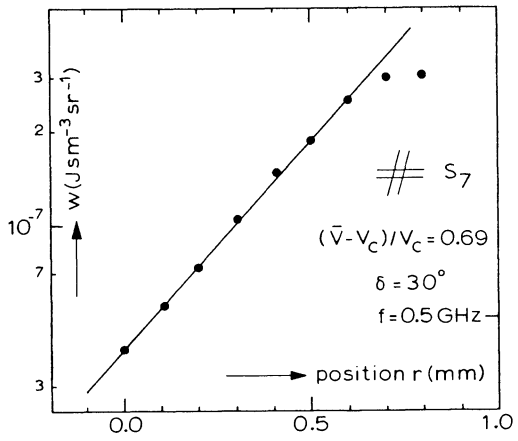

Fig. 7. The spectral acoustic-energy density for $\delta = 30°$ at 0.5 GHz versus position. The position vector was in the direction of the associated acoustic group velocity (at 45°). The origin was chosen arbitrarily.

the net attenuation coefficient α_N calculated before. With the help of these experimental results we were able to estimate by extrapolation the spectral acoustic-energy density at positions near the cathode. Near the cathode we found $w/w_{th} \simeq 3 \times 10^3$ (for comparison, near the anode $w/w_{th} \simeq 4 \times 10^6$). This result indicates that net round-trip gain occurred in the sample during the build-up of the acoustic flux. Net round-trip gain has been observed before in CdS by Hutson et al. [44] and McFee [45]. Finally a stationary state will be reached when the net round-trip gain is reduced to unity due to some nonlinear loss mechanism.

Fig. 8 shows w/w_{th} plotted versus frequency for sample s_3 at different applied voltages. The values of the reduced voltage $(\bar{V} - V_c)/V_c$ have been indicated. Note that the dimensionless quantity w/w_{th} is proportional to w/f^2 (cf. eq. (20)). We observe that the acoustic-energy density increases with increasing voltage. Maxima in the spectra occur at frequencies much lower than predicted by White's theory (according to White's theory $f_m \simeq 1.3$ GHz). In addition, these maxima are found to shift towards lower frequencies with increasing voltage. Notice that the broadening of the spectra with increasing voltage is apparent rather than real due to the

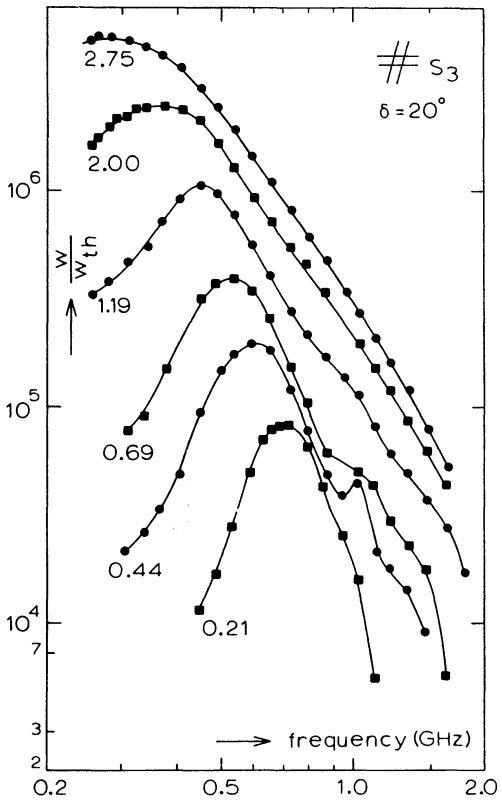

Fig. 8. The relative spectral acoustic-energy density w/w_{th} versus frequency at different applied voltages for sample s_3. The values of the reduced voltage $(\bar{V}-V_c)/V_c$ have been indicated; V_c is the voltage marking the onset of electro-acoustic current fluctuations. The off-axis angle was 20°.

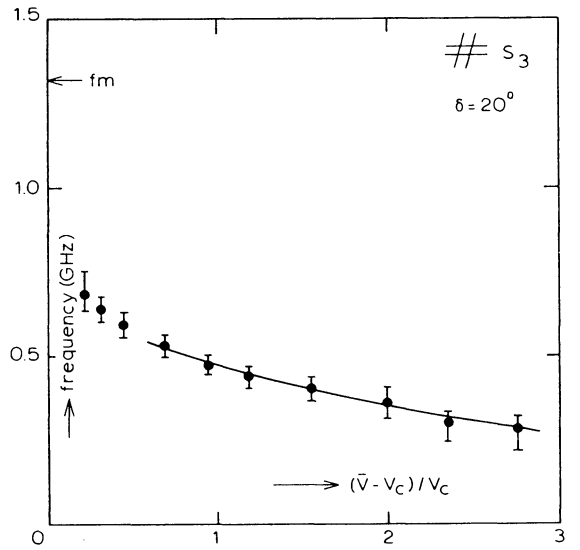

Fig. 9. Frequencies of maximum w/w_{th} versus the reduced voltage (dots) for sample s_3. The off-axis angle was 20°. The solid line corresponds to maxima in the net amplification coefficient, if $s = 1.0\,\mu m$ is used (s is a measure for the surface-flatness of the crystal side-faces). The frequency of maximum amplification according to the theory of White has been indicated with an arrow on the vertical scale.

logarithmic frequency scale. The curve at $(\bar{V}-V_c)/V_c = 0.44$ shows a small additional maximum around 1 GHz. With increasing voltage this maximum turns into a small shoulder and finally it is no longer observable. Possibly this additional maximum may be interpreted as a peak left over from the early growth-stage of the acoustic flux: during the early growth-stage the amplification can be assumed to peak around a frequency close to that predicted by White's theory [5–12]; in our case $f_m \simeq 1.3$ GHz.

In fig. 9 the frequencies corresponding to the principal maxima in w/w_{th} (cf. fig. 8) have been plotted versus the reduced voltage for sample s_3 (black dots). The solid line was calculated from maxima in the net amplification coefficient $-\alpha_N$ (cf. eq. (6)) by putting $s = 1.0\,\mu m$, which again is quite an acceptable value. Note that the adjusted parameter s, because it takes account of boundary-scattering losses only, should be independent of the applied voltage. Therefore the voltage dependence of the frequency of maximum net amplification essentially arises from the voltage dependence of the electro-acoustic amplification coefficient $-\alpha_e$ (cf. eq. (2)). The voltage dependence of the latter is determined by the drift parameter (cf. eq. (2)), and the ac-impedance plateau value (cf. eq. (1)). For $(\bar{V}-V_c)/V_c \lesssim 0.6$ the calculation of α_N becomes very inaccurate, because α_e and $(\alpha_L + \alpha_S)$ are almost of the same magnitude and have opposite signs (cf. eq. (6)).

It should be noted that when the reduction of the conductivity was neglected (replacing σ_1 by the Ohmic conductivity) no acceptable curve could be fitted to the data of fig. 9 with the help of eq. (6).

We conclude that the down-shift of the

frequency of maximum amplification can be described quite reasonably by the linear theory, if a reduction in the conductivity, and the acoustic losses due to boundary scattering are taken into account.

From measurements of the spectral acoustic-energy distribution for sample s_3 as a function of position we again found, as in the case of sample s_7, an exponential position-dependence. The thus obtained operationally defined amplification coefficients have been plotted in fig. 10 versus the reduced voltage (black dots). The data were taken at the frequencies where the ratio w/w_{th} reaches a maximum (cf. fig. 8). The solid line represents the calculated net amplification coefficient, $-\alpha_N$, again using $s = 1.0\ \mu m$. We conclude that the calculated net amplification coefficient α_N is indicative only for the order of magnitude of the operationally defined amplification coefficient which was determined from the spatial distribution of the stationary acoustic flux. There is no quantitative agreement. However, it is not clear whether we should expect such agreement. The agreement between these two amplification coefficients as found for sample s_7 (cf. fig. 7) can be regarded as accidental.

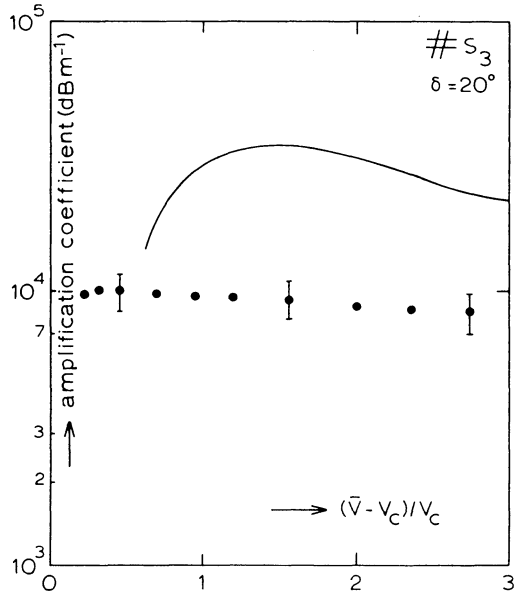

Fig. 10. The operationally defined amplification coefficient for sample s_3, obtained from measurements of the spatial distribution of the acoustic energy at frequencies of maximum w/w_{th}, as a function of the reduced voltage $(\bar{V} - V_c)/V_c$ (dots). The solid line represents the calculated net amplification coefficient $-\alpha_N$, at frequencies of maximum amplification (putting $s = 1.0\ \mu m$).

Fig. 11 shows acoustic spectra for sample s_4 at different applied voltages. The values of the reduced voltage $(\bar{V} - V_c)/V_c$ have been indicated. Again a pronounced down-shift is observed with increasing voltage. At voltages relatively close to the critical voltage V_c a small, additional maximum is observed, which becomes a shoulder at higher voltages. This second maximum at $(\bar{V} - V_c)/V_c = 0.23$ is found to be located close to the frequency of maximum am-

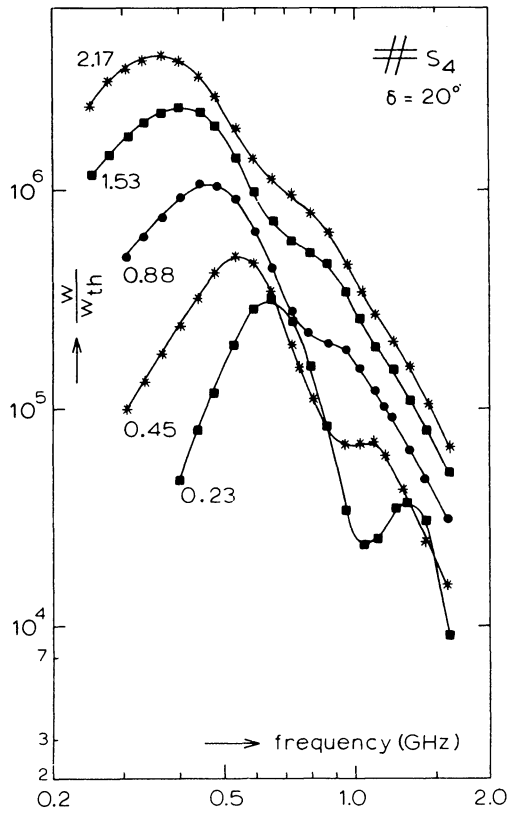

Fig. 11. The relative spectral acoustic-energy density w/w_{th} versus frequency at different applied voltages for sample s_4. The values of the reduced voltage $(\bar{V} - V_c)/V_c$ have been indicated. The off-axis angle was 20°.

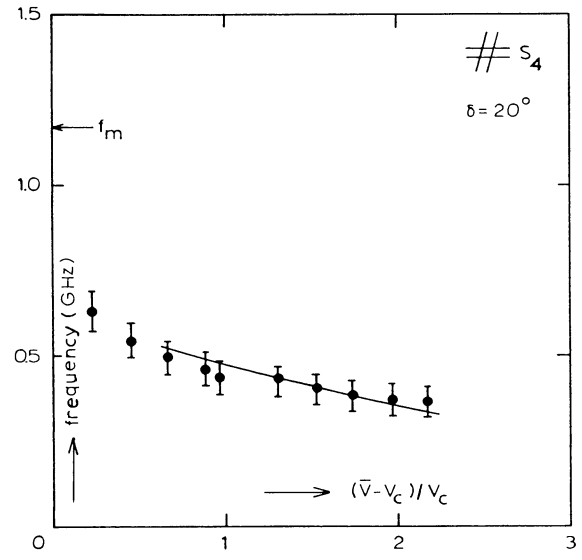

Fig. 12. Experimental frequencies of maximum w/w_{th} versus the reduced voltage (dots) for sample s_4. The off-axis angle was 20°. The solid line corresponds to maxima in the net amplification coefficient, calculated if $s = 0.9$ μm is used. The frequency f_m of maximum amplification, according to the theory of White has been indicated by an arrow on the vertical scale.

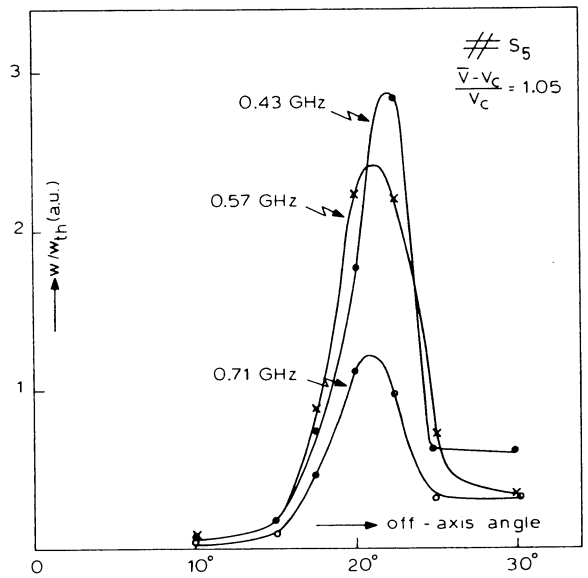

Fig. 13. The angular distribution of the relative spectral acoustic-energy density for sample s_5 at $(\bar{V} - V_c)/V_c = 1.05$ for three different frequencies. The solid lines have been drawn to guide the eye.

plification that follows from White's theory, if the Ohmic conductivity is used ($f_m \approx 1.2$ GHz).

In fig. 12 the frequencies corresponding to the principal maxima in w/w_{th} (cf. fig. 11) have been plotted versus the reduced voltage for sample s_4. The solid line was calculated from maxima in the net amplification coefficient $-\alpha_N$ (cf. eq. (6)) by putting $s = 0.9$ μm.

Measurements of the angular distribution of the acoustic-energy density for sample s_5 at $(\bar{V} - V_c)/V_c = 1.05$ are shown in fig. 13. The solid lines have been drawn to guide the eye. The important feature of these experimental data is that the acoustic-energy density peaks at an off-axis angle of about 20°. As we pointed out before information about the angular distribution of the acoustic-energy density can also be obtained from resonance frequencies occurring in the ac impedance. Fig. 14 shows the absolute value $|Z|$ of the ac impedance as measured for sample s_5 at $(\bar{V} - V_c)/V_c = 1.05$. For details about the measuring procedure the reader is referred to [23]. Apparently, the maxima in the ac impedance coincide with the odd harmonics of $(2.8 \pm 0.1) \times 10^5$ Hz. As we pointed out before

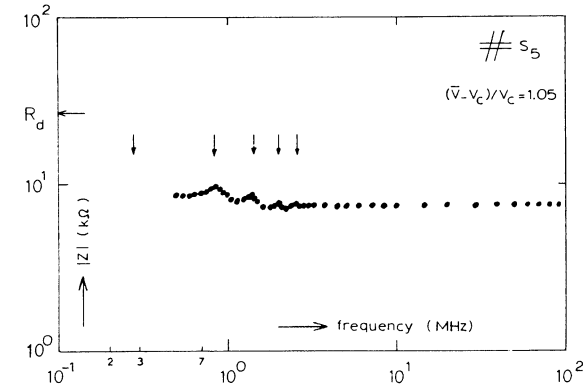

Fig. 14. The absolute value of the ac impedance Z as a function of frequency for sample s_5 at $(\bar{V} - V_c)/V_c = 1.05$. The value of the differential resistance R_d has been indicated by a horizontal arrow on the vertical scale. The vertical arrows correspond to odd harmonics of 2.8×10^5 Hz.

[21, 23], these maxima can be related to the group velocity of the amplified acoustic waves (cf. eq. (7)). Using eq. (7) we obtained for the component of the group velocity along the c-axis $v_{g_3} = (1.56 \pm 0.06) \times 10^3$ m s^{-1}. From this result and with the help of the known elastic constants [46, 47] we found the off-axis angle of the associated acoustic waves to be $\delta = 22° \pm 5°$. We conclude that this result is in good agreement with the off-axis angle of maximum acoustic-energy density as obtained from fig. 13. This indicates that, as proposed before [23], the determination of resonance frequencies in the ac impedance is a useful tool for finding the off-axis angle of maximum acoustic-energy density.

5. Conclusion

Brillouin-scattering studies of the stationary electro-acoustically amplified acoustic flux showed that the acoustic spectra peak at frequencies which could be as much as 4 times lower than those predicted by White's linear theory [17]. The frequencies of maximum acoustic-energy density were found to be independent of position. With increasing voltage the acoustic energy was found to increase; the frequencies of maximum acoustic energy were found to shift towards lower frequencies. If the effects of acoustic scattering-losses at the crystal side-faces, and a reduction of the conductivity are taken into account, this down-shift could be described by the linear theory. However, the calculated amplification coefficients appeared to be indicative only of the order of magnitude of the operationally defined amplification coefficients that were obtained from the spatial distribution of the acoustic energy.

The off-axis angle of maximum acoustic-energy density as obtained from Brillouin-scattering experiments appeared to be in good agreement with the off-axis angle as calculated from resonance frequencies in the ac impedance.

Acknowledgements

The author is very grateful to Prof. R.J.J. Zijlstra and to Prof. C.Th.J. Alkemade for their critical reading of the manuscript and their valuable suggestions and comments. This work is part of the research program of the Stichting voor Fundamenteel Onderzoek der Materie (Foundation for Fundamental Research on Matter) and was made possible by financial support from the Nederlandse Organisatie voor Zuiver-Wetenschappelijk Onderzoek (Netherlands Organization for the Advancement of Pure Research).

References

[1] J. Zucker and S. Zemon, Appl. Phys. Lett. 9 (1966) 398.
[2] S. Zemon, J.H. Wasko, L.L. Hope and J. Zucker, Appl. Phys. Lett. 11 (1967) 40.
[3] S. Zemon, J. Zucker, J.H. Wasko, E.M. Conwell and A.K. Ganguly, Appl. Phys. Lett. (1968) 378.
[4] J. Zucker and S. Zemon, J. Ac. Soc. Am. 49 (1971) 1037.
[5] B.W. Hakki and R.W. Dixon, Appl. Phys. Lett. 14 (1969) 185.
[6] M. Bruun, W. Wettling and N.I. Meyer, Phys. Lett. 31A (1970) 31.
[7] D.L. Spears, Phys. Rev. B2 (1970) 1931.
[8] A. Many and U. Gelbart, Appl. Phys. Lett. 19 (1971) 192.
[9] U. Gelbart and A. Many, Phys. Rev. B7 (1973) 2713.
[10] M. Yamada, C. Hamaguchi and J. Nakai, J. Phys. Soc. Japan 33 (1972) 865.
[11] M. Yamada, C. Hamaguchi, K. Matsumoto and J. Nakai, Phys. Rev. B7 (1973) 2682.
[12] M. Yamada, C. Hamaguchi, J. Phys. Soc. Japan 36 (1974) 747.
[13] M. San'ya, M. Yamada, C. Hamaguchi and J. Nakai, Jpn. J. Appl. Phys. 13 (1974) 611.
[14] J. Attal and J.P. Laurenti, J. Phys. C: Sol. St. Phys. 7 (1974) 1160.
[15] O. Keller, Phys. Rev. B10 (1974) 1585.
[16] O. Keller, Phys. Rev. B11 (1975) 5059.
[17] D.L. White, J. Appl. Phys. 33 (1962) 2547.
[18] M.B.N. Butler, Rep. Prog. Phys. 37 (1974) 421.
[19] R.W. Smith, Phys. Rev. Lett. 9 (1962) 87.
[20] A.R. Moore, J. Appl. Phys. 38 (1967) 2327.
[21] W. Westera, Physica 113B (1982) 149.
[22] W. Westera, Physica B (1982) to be published.
[23] W. Westera, Physica 113B (1982) 284.
[24] N.I. Meyer and M.H. Jørgensen, in Festkörperprobleme X, ed. O. Madelung (Pergamon, Vieweg, 1970) p. 21.

[25] A.R. Moore, R.W. Smith and P. Worcester, IBM J. Res. Developm. 13 (1969) 503.
[26] T.B. Bateman and J.H. McFee, J. Appl. Phys. 39 (1968) 4471.
[27] F. Siebert, O. Keller and W. Wettling, Phys. Stat. Sol. (a) 4 (1971) 67.
[28] O. Keller, Phys. Lett. 39A (1972) 235.
[29] S. Furukawa and T. Hata, El. Comm. Japan. 54C (1971) 118.
[30] T. Hata, T. Nakano, K. Koma and T. Hada, Appl. Phys. Lett. 33 (1978) 3.
[31] Y. Tokunaga, T. Hata, Y. Neda and T. Hada, Jpn. J. Appl. Phys. 19 (1980) 379.
[32] A. Akhiezer, J. Phys. 1 (1939) 277 (in Russian).
[33] B.J. Berne and R. Pecora, Dynamic Light Scattering (Wiley, New York, 1975).
[34] W. Hayes and R. Loudon, Scattering of Light by Crystals (Wiley, New York, 1978).
[35] L. Landau and G. Placzek, Fysik Z. Sowj, 5 (1934) 172.
[36] G.B. Benedek and K. Fritsch, Phys. Rev. B149 (1966) 647.
[37] L. Brillouin, Ann. Phys. (Paris) 17 (1922) 88.
[38] E. Gross, Nature 126 (1930) 201, 400, 603.
[39] R.W. Dixon, IEEE J. Quant. El. QE-3 (1967) 85.
[40] C. Hamaguchi, J. Phys. Soc. Japan 35 (1973) 832.
[41] S. Mishra and R. Bray, Sol. St. Comm. 33 (1980) 281.
[42] M. Born and E. Wolf, Principles of Optics (Pergamon, Oxford, 1970).
[43] K. Ando and C. Hamaguchi, Phys. Rev. B11 (1975) 3876.
[44] A.R. Hutson, J.H. McFee and D.L. White, Phys. Rev. Lett. 7 (1961) 237.
[45] J.H. McFee, J. Appl. Phys. 34 (1963) 1548.
[46] D. Berlincourt, H. Jaffe and L.R. Shiozawa, Phys. Rev. 129 (1963) 1009.
[47] I.B. Kobiakov, Sol. State Commun. 35 (1980) 305.